Available online at www.sciencedirect.com

ScienceDirect

Procedia CIRP 101 (2021) 30–33

www.elsevier.com/locate/procedia

9th CIRP Conference on High Performance Cutting (HPC 2020)

Anisotropy effect on Laser Powder Bed Fused Ti6Al4V machinability

Lucia Lizzul[a]*, Marco Sorgato[a], Rachele Bertolini[a], Andrea Ghiotti[a], Stefania Bruschi[a]

[a]*Department of Industrial Engineering, University of Padova, Via Venezia 1, 35131, Padova, Italy*

* Corresponding author. Tel.: 049-827 6819; *E-mail address:* lucia.lizzul@phd.unipd.it

Abstract

Final machining steps are commonly requested on parts obtained via additive manufacturing to ensure the required surface finish and geometrical tolerances. When machining additive manufactured workpieces, their typical microstructural anisotropy is rarely taken into consideration. In this work, the influence of the build-up orientation of Ti6Al4V parts obtained via laser powder bed fusion on machinability is studied. Ti6Al4V blocks with horizontal and vertical development were additively manufactured and then milled. Tool wear progression was monitored and its effect on surface quality investigated. The cutting tool that machined the horizontally oriented sample showed a tool life 66% higher than the one that machined the vertically oriented one. This study demonstrates the strong correlation between the build-up orientation of additive manufactured components and their machining response.

Keywords: Titanium; Additive Manufacturing; Milling; Wear; Surface integrity

1. Introduction

With Additive Manufacturing (AM) technologies it is not always possible to obtain the surface finish and geometrical tolerances suitable for the final purpose of the part. This requires a machining step in the process chain to get the final product. However, the machinability of the AM metals is not yet fully characterized due to the complexity of their microstructure. In fact, each powder deposit undergoes a different thermal history, leading to a different microstructure along the part height, depending also on its build-up orientation with respect to the base plate [1,2]. The typical heat treatments carried out on the AM components do not remove the directionality of the microstructure [3], and this has been proven to influence the mechanical properties of AM parts [4] and an impact on their machinability is as well expected. Few literature studies take into consideration the close correlation between anisotropy of metal AM parts and their machinability, especially in terms of tool wear [5,6]. As for the Ti6Al4V alloy, most of the works concern turning operation and none of them gives guidelines to describe the observed phenomena [7,8]. The present work studies the influence of the build-up orientation of AM Ti6Al4V parts on their machinability. To this end, Laser Powder Bed Fused (LPBF) Ti6Al4V blocks were produced with both horizontal and vertical developments, heat treated and finally end milled. Usually, AM components are small-sized parts that need to be finished with high dimensional accuracy that can be achieved and guaranteed by small-diameter cutting tools. Hence, a small diameter tool was chosen for the experimental trials and the tool diameter reduction was periodically monitored and analyzed, along with the chips produced. Moreover, the quality of the resulting machined surfaces was investigated in terms of burrs formation, surface roughness, and defects. The outcomes confirmed the correlation between the anisotropy of the AM parts and their machinability, representing a starting point for a comprehensive analysis of the AM metals response to machining.

10.1016/j.procir.2021.02.006

2. Experimental

The machining tests were carried out on LPBF Ti6Al4V (grade 5) samples manufactured using the MYSINT100 SISMA™ machine, starting from a plasma-atomized Ti6Al4V powder (15-45 µm) supplied by LPW Technology™. Two blocks measuring 15 × 30 × 10 mm^3 were built up with Horizontal Orientation (HO) and Vertical Orientation (VO) with respect to the base platform, using the island scanning strategy. The laser had a power of 105 W with a spot diameter of 30 µm. The scanning speed was set to 1200 mm/s, while the hatch spacing and layer thickness were 80 µm and 20 µm, respectively. To relieve residual stresses and improve mechanical properties by stabilizing the microstructure and closing the porosities [9], the LPBF samples underwent a subtransus heat treatment prior to the cutting tests. The heat treatment was conducted at 950°C for 30 min under a protecting argon atmosphere followed by furnace cooling in the Carbolite Gero™ RHF laboratory furnace. Fully dense parts (density > 99.9% ± 0.3%) were thus obtained. The microstructure of the LPBF Ti6Al4V pieces was inspected via the Leica™ DMRE optical microscope. The samples were sectioned at the same height from the base platform to reduce the differences caused by the thermal gradient along the deposited layers, which is known to greatly affect the microstructure. The samples for the metallographic examination were ground with sandpapers and polished using colloidal silica mixed with hydrogen peroxide. To reveal the microstructure the Kroll's reagent was used. The measurements of the microstructural features were performed using Matlab™ on six micrographs at different magnifications. The Vickers microhardness of the samples was measured with the Leitz™ Durimet tester with a load of 100 g according to ASTM E92 [10]. Three series of ten indentations were casually distributed on the face C (refer to Fig. 2) of both the samples, perpendicularly to the face A, the one that was machined afterward. The microhardness average value was calculated and reported in Fig. 2.

Machining operations were conducted with the ultra-precision micro-milling machine Kugler™ Micromaster 5X under Minimum Quantity Lubrication (MQL) conditions. The natural-based oil Accu-Lube™ LB 5000 was utilized as lubricant and sprayed onto the cutting zone at 150 ml/h of flow rate and 0.70 MPa of air pressure. The utilized cutting tool was the CoroMill® Plura end mill 2P121-0200-NC grade H10F by Sandvik™ Coromant. The end mill was made of uncoated tungsten carbide, double fluted, with 2 mm of diameter and 0.15 mm of corner radius. The experimental set-up is displayed in Fig. 1.

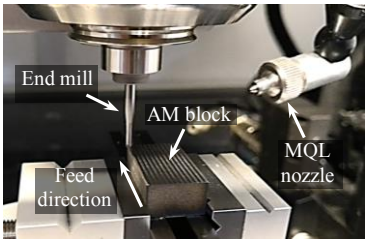

Fig. 1. Machining test setup.

The tools were inspected with a FEI™ Quanta 400 Scanning Electron Microscope (SEM) to ascertain the absence of production defects before the use and one fresh end mill was employed for each block. The machining trials consisted of a series of full immersion slots machined over a length of 20 mm on the face A of both the blocks, which was previously flattened by grinding (See Fig. 2). The axial depth of cut was 0.2 mm, the cutting speed and the feed per tooth, which were selected from the tool manufacturer's datasheet, were 75 m/min and 0.02 mm/tooth, respectively.

To examine the influence of the build-up orientation of the LPBF Ti6Al4V samples on their machinability, the tool wear and the resulting surfaces were analyzed after each planned cutting time (i.e. 0.4 min), until they catastrophically failed. Because of the reduced dimensions of the employed cutting tool, and the difficulty of applying the standard methods for tool wear evaluation, the tool wear was assessed referring to a criterion used in micro-milling, namely the tool diameter reduction, which was measured from SEM images, in agreement with [11,12]. One test run was considered sufficient based on preliminary tests and literature findings, cited through the paper. The arithmetical mean height of the scale-limited surface (*Sa*) was measured at the center of the slot using the Sensofar™ PLu-Neox optical profiler with a 20× Nikon™ confocal objective, according to ISO 25178-1 [13]. Machined surface defects, burrs, and chips morphology were analyzed using the SEM.

3. Experimental results and discussion

3.1. Microstructural anisotropy of LPBF Ti6Al4V

Fig. 2 reports the LPBF Ti6Al4V blocks configuration and their cross-sectional microstructure after the heat treatment. Long prior β grains developed along the Z axis with continuous α phase layers at their boundaries and α phase (in light) and β phase (in dark) lamellae lying within it, as reported also by Vrancken et al. [9]. The different prior β grains orientation and size reported in Fig. 2 is related to the thermal gradient developing in the AM part. In fact, the β grains grow along the direction of the higher thermal gradient during the AM process, that is the build-up direction. Moreover, lower cooling rates lead to wider β grains [1,2], thus HO and VO samples experienced similar cooling rates at the analyzed height since comparable β grains widths were found.

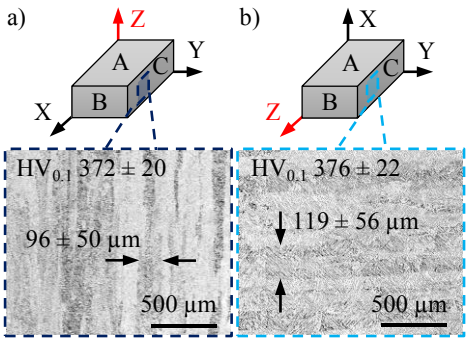

Fig. 2. LPFB Ti6Al4V lateral microstructures of the a) HO and b) VO samples. The build-up direction is along the Z axis, highlighted in red. Microhardness and prior β grains width are also reported.

3.2. Tool wear

Fig. 3 shows the tool diameter reduction for the two LPFB samples as a function of the cutting time. The time at which Catastrophic Failure (CF) occurred is also reported. The different trend of the curves clearly shows the effect of the build-up orientation. In particular, the end mill that machined the HO sample showed a tool life 66% higher than the one that machined the VO one. Fig. 4 reports the virgin cutting tools in the background with zoomed pictures of worn edges at the last monitored cutting time step of the two samples. The worse condition of the end mill that machined the VO sample is observable. To explain the difference in the tool wear, the following considerations on the sample microstructure have to be made. As described in Section 3.1, after the heat treatment, α phase layers form along the grain boundaries of the β grains, acting as material discontinuity zones, along which fracture preferentially occurs [1,4]. These weak zones may favor the material removal during cutting if favorably oriented with respect to the cutting edge. In the HO sample, the prior β grains, so the α phase layers, are parallel to the end mill axis, thus to the entering angle of the cutting tool (~ 90°). In the case of the VO sample, the α phase layers are orthogonal to the entering angle of the end mill, resulting irrelevant in the cutting process. According to this, the tool wear when machining the HO sample should be lower compared to that when machining the VO one, as actually occurred. The main observed tool wear phenomena were adhesion, attrition, and abrasion. Adhesive wear was the predominant one, according to what reported in literature for titanium alloys by Ulutan and Ozel [14]. Attrition led to flaking and stair-formed face wear, while abrasion was the principal cause of the tool diameter reduction. All the above-mentioned phenomena occurred mainly in the VO sample, in agreement with what stated before.

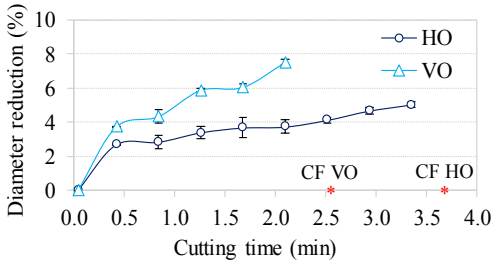

Fig. 3. Variation of the tool diameter as a function of the cutting time.

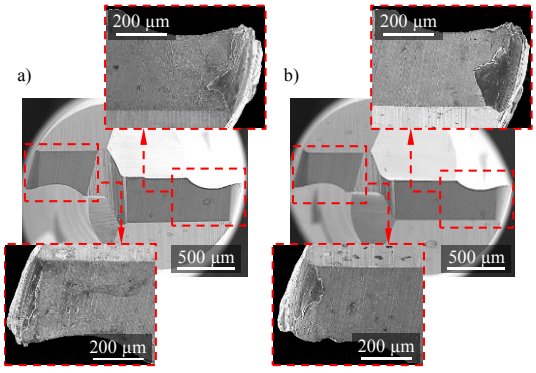

Fig. 4. Virgin cutting tools in the background with zoomed edges showing wear at the last monitored cutting time of a) HO sample and b) VO sample.

3.3. Chip morphology

For both the samples, curled and faint serrated chips were obtained (Fig. 5 a) and b)). The contact surface of the chips with the tool rake face was quite smooth, with slight scratches along the chip length caused by the hard particles of the tool rake face. Regardless of the machined sample, the chip thickness progressively increased from the ends to the center, according to the slotting dynamics. The chip length corresponded to the width of the slot, while the chip width was higher than the axial depth of cut due to the compression action of the tool rake face in the cutting direction. Analyzing the swarf at a higher magnification, a distinction between the chips produced machining the two samples was observed. In Fig. 5 c) and d) the chip thickness at the chip center is shown: it is slightly higher in the case of the VO sample with respect to the HO one, meaning that the chip compression ratio in the case of the VO sample is higher, hence higher the cutting power [15]. Consequently, the shear plane angle Φ at the primary shear zone, highlighted in Fig. 5 c) and d), is lower for the VO sample, which is an index of higher cutting forces [16]. These observations agree with the tool wear results, being the VO sample machinability lower. When the tool wear reached an advanced state, large shear plastic deformation took place leading to shorter chips with extended cracks, moreover, serration occurred. The chip contact surface presented large protrusions because of missing tool material that created dimples on the tool cutting edge.

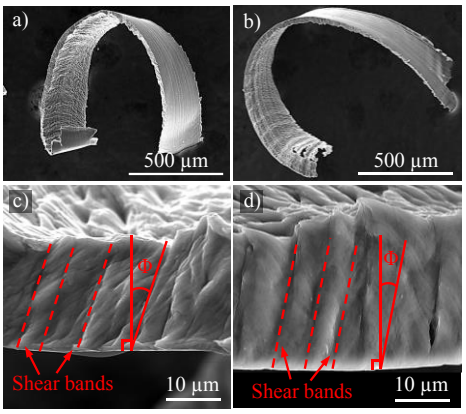

Fig. 5. Chip morphology a)-b) and thickness c)-d) at the beginning of the milling tests carried out on the HO sample and VO sample, respectively.

3.4. Surface quality

The machined slots at the first and last monitoring step for the two samples are shown in Fig. 6. It can be observed that the burrs at the beginning of the milling tests were absent, while at the last stage of tool life they were very evident, mainly in the down-milling side as found by Zheng et al. [17]. The burrs extent was higher for the VO sample compared to the HO one, in agreement with the tool wear outcomes. The surface roughness *Sa* trends are reported in Fig. 7. At the first machined slot, the *Sa* value of the VO sample was 10% higher than the one of the HO sample. This relies on the different machinability of the two samples as explained in Section 3.2, rather than on the difference in microhardness, which was negligible. When the tool wear reached an advanced state, *Sa*

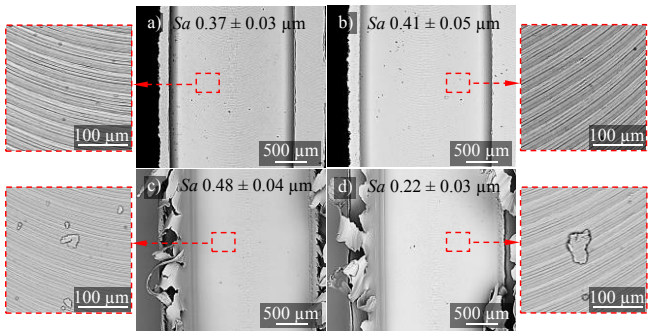

Fig. 6. Burrs morphology and zoomed pictures of the machined surface at the first a)-b), and last c)-d) slots of the HO and VO samples, respectively.

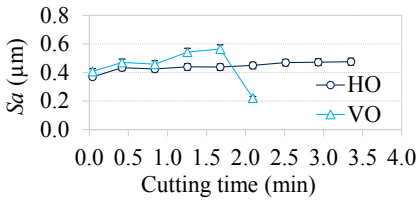

Figure 7. Surface roughness trends as a function of the cutting time.

increased for the HO sample, but greatly diminished for the VO one. Normally, when the tool wear increases, the surface roughness increases, however, when the cutting edges are greatly damaged, so as to increase the cutting edge radius, the cutting mechanism changes from shearing to plowing and the machined surface roughness may diminish. This is in accordance with the worse cutting edge status of the tool that machined the VO sample compared to the one that machined the HO sample (Fig. 4). At the beginning of the milling operations, surface defects were barely present (see Fig. 6): mainly feed marks with slight smearing and rare particles of adhered material were detected. As the tool wear increased, feed marks became smeared and adhered material was found to be more frequent, located mainly on the sides of the slot. This may be due to the higher cutting forces and temperatures that generally rise when the tool wear reaches the last wear stage before the CF [18]. In particular, the VO sample was characterized by a higher amount of defects because of the higher tool wear.

4. Conclusions

In this paper, the impact of the build-up orientations of LPBF Ti6Al4V parts on machinability was assessed. Two blocks with horizontal and vertical orientations were end milled under MQL conditions, monitoring the tool diameter reduction. The results confirm the influence of the AM parts build-up orientation on the microstructural anisotropy, which, in turn, influences the machinability. The main findings are:

- The build-up orientation affected the prior β grains development.
- The VO sample induced higher tool wear compared to the HO one because of the influence of the AM microstructural features developed with the heat treatment.
- The AM microstructural features influenced the surface roughness, which was higher for the VO sample and augmented in line with the tool wear.
- The chip morphology was found to comply with the tool wear, being the shear plane angle of the chips of the VO sample lower than the one of the chips of the HO sample.

Acknowledgments

The authors wish to express their gratitude to Antonio Tarallo of Sandvik Italia S.p.A. for providing the tools and SISMA S.p.A., which manufactured the AM samples.

References

[1] de Formanoir C, Michotte S, Rigo O, Germain L, Godet S. Electron beam melted Ti-6Al-4V: Microstructure, texture and mechanical behavior of the as-built and heat-treated material. Mater Sci Eng A 2016;652:105–19.
[2] Sharma H, Parfitt D, Syed AK, Wimpenny D, Muzangaza E, Baxter G, et al. A critical evaluation of the microstructural gradient along the build direction in electron beam melted Ti-6Al-4V alloy. Mater Sci Eng A 2019;744:182–94.
[3] Chastand V, Tezenas A, Cadoret Y, Quaegebeur P, Maia W, Charkaluk E. Fatigue characterization of Titanium Ti-6Al-4V samples produced by Additive Manufacturing. Procedia Struct Integr 2016;2:3168–76.
[4] Simonelli M, Tse YY, Tuck C. Effect of the build orientation on the mechanical properties and fracture modes of SLM Ti-6Al-4V. Mater Sci Eng A 2014;616:1–11.
[5] Fernandez-Zelaia P, Nguyen V, Zhang H, Kumar A, Melkote SN. The effects of material anisotropy on secondary processing of additively manufactured CoCrMo. Addit Manuf 2019;29:100764.
[6] Hojati F, Daneshi A, Soltani B, Azarhoushang B, Biermann D. Study on machinability of additively manufactured and conventional titanium alloys in micro-milling process. Precis Eng 2020;62:1–9.
[7] Shunmugavel M, Polishetty A, Goldberg M, Littlefair G. Tool Wear and Surface Integrity Analysis of Machined Heat Treated Selective Laser Melted Ti-6Al-4V. Int J Mater Form Mach Process 2016;3.
[8] Sartori S, Bordin A, Moro L, Ghiotti A, Bruschi S. The Influence of Material Properties on the Tool Crater Wear When Machining Ti6Al4 v Produced by Additive Manufacturing Technologies. Procedia CIRP 2016;46:587–90.
[9] Vrancken B, Thijs L, Kruth JP, Van Humbeeck J. Heat treatment of Ti6Al4V produced by Selective Laser Melting: Microstructure and mechanical properties. J Alloys Compd 2012;541:177–85.
[10] ASTM E92: Standard Test Methods for Vickers Hardness and Knoop Hardness of Metallic Materials.
[11] Ucun I, Aslantas K, Bedir F. An experimental investigation of the effect of coating material on tool wear in micro milling of Inconel 718 superalloy. Wear 2013;300:8–19.
[12] Sorgato M, Bertolini R, Bruschi S. On the correlation between surface quality and tool wear in micro–milling of pure copper. J Manuf Process 2020;50:547–60.
[13] ISO 25178-1: Surface texture: Areal Part 1: Indication of surface texture.
[14] Ulutan D, Ozel T. Machining induced surface integrity in titanium and nickel alloys : A review. Int J Mach Tools Manuf 2011;51:250–80.
[15] Astakhov VP, Shvets S. The assessment of plastic deformation in metal cutting. J Mater Process Technol 2004;146:193–202.
[16] Grzesik W. Prediction of the Functional Performance of Machined Components Based on Surface Topography: State of the Art. J Mater Eng Perform 2016;25:4460–8.
[17] Zheng L, Chen W, Huo D. Experimental investigation on burr formation in vibration-assisted micro-milling of Ti-6Al-4V. Proc Inst Mech Eng Part C J Mech Eng Sci 2019;233:4112–9.
[18] Brinksmeier E, Preuss W, Riemer O, Rentsch R. Cutting forces, tool wear and surface finish in high speed diamond machining. Precis Eng 2017;49:293–304.